Radio-Frequency Reflectometry in Bilayer Graphene Devices Utilizing Microscale Graphite Back-Gates

Tomoya Johmen,[1,2] Motoya Shinozaki,[1,2,3] Yoshihiro Fujiwara,[1,2] Takumi Aizawa,[1,2] and Tomohiro Otsuka[1,2,3,4,5,*]

[1] *Research Institute of Electrical Communication, Tohoku University, 2-1-1 Katahira, Aoba-ku, Sendai 980-8577, Japan*

[2] *Graduate School of Engineering, Tohoku University, 6-6 Aramaki Aza Aoba, Aoba-ku, Sendai 980-0845, Japan*

[3] *WPI Advanced Institute for Materials Research, Tohoku University, 2-1-1 Katahira, Aoba-ku, Sendai 980-8577, Japan*

[4] *Center for Science and Innovation in Spintronics, Tohoku University, 2-1-1 Katahira, Aoba-ku, Sendai 980-8577, Japan*

[5] *Center for Emergent Matter Science, RIKEN, 2-1 Hirosawa, Wako, Saitama 351-0198, Japan*

(Received 10 January 2023; revised 12 April 2023; accepted 20 June 2023; published 17 July 2023)

Bilayer graphene is an attractive material that hosts a high-quality two-dimensional electron gas with a controllable band gap. By utilizing the band gap, electrical gate tuning of the carrier is possible and formation of nanostructures such as quantum dots has been reported. To probe the dynamics of the electronic states and realize applications for quantum bit devices, radio-frequency (rf) reflectometry, which enables high-speed electrical measurements, is important. Here we demonstrate rf reflectometry in bilayer graphene devices. We utilize a microscale graphite back-gate and an undoped Si substrate to reduce the parasitic capacitance, which degrades the rf reflectometry measurement. We measure the resonance properties including the matching condition of a tank circuit, which contains the bilayer graphene device. We construct a demodulated rf reflectometry setup and compare the result with dc measurement, and confirm their consistency. The wide-range frequency-dependent noise behavior is also analyzed. From the noise analysis, we calculate the readout error rate of our device for single-electron detection and demonstrate that a vertically integrated charge sensor has the potential to achieve a low error rate. We also measure Coulomb diamonds of quantum dots possibly formed by bubbles and confirm that rf reflectometry of quantum dots can be performed. This technique enables high-speed measurements of bilayer graphene quantum dots and contributes to the study of bilayer-graphene-based quantum devices by fast readout of the states.

DOI: 10.1103/PhysRevApplied.20.014035

I. INTRODUCTION

Bilayer graphene (BLG) is a member of the family of nanocarbon materials, which has attracted attention for its unique properties [1,2]. The properties of BLG, including the formation of quantum dots, have been intensively studied [3–11]. Quantum dots [12–15] are nowadays essential elements in semiconductor spin quantum bits [16–22] and electronic sensors [23–25]. BLG has the potential to improve their performance by utilizing the weak spin-orbit interaction and decreasing the nuclear spins [26]. Also, BLG has a nontrivial topological band, resulting in the charge carriers acquiring a Berry phase providing many fascinating characteristics [27–30]. Therefore, it is expected to be a good platform for valleytronics.

For BLG, most of reports directly measure the current flowing through the quantum dots with low-frequency electronics. To access the faster dynamics of the electronic states and for applications to quantum bits, faster and more sensitive electronic measurements are required. In order to realize this faster readout, radio-frequency (rf) reflectometry is a powerful tool to improve the measurement bandwidth [31–35]. This technique applies rf signals to resonators including target devices and monitors the reflected rf signals. The impedance of the target devices can be monitored through the reflected signals. In this measurement setup, we need to decrease the stray capacitance in the measurement circuit to reduce rf leakage and optimize the properties of the resonators. However, in conventional BLG devices on SiO_2 and highly doped Si back-gates, large stray capacitances are formed by the device electrodes and the back-gates.

*tomohiro.otsuka@tohoku.ac.jp

 © 2023 American Physical Society

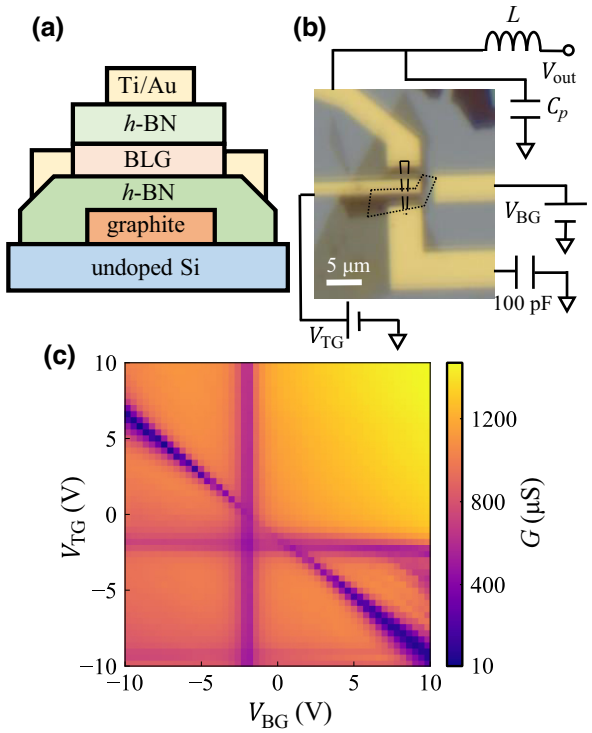

FIG. 1. (a) Layer structure of the device. The two-dimensional electron gas is formed in the bilayer graphene, which is connected to Ti/Au. The thicknesses of the top and bottom hexagonal boron nitride layers are 18 and 25 nm confirmed by atomic force microscopy, respectively. (b) Optical microscope image of the device and schematic of the measurement setup. An rf tank circuit is connected to the source of the device. (c) Observed conductance of the bilayer graphene as a function of V_{TG} and V_{BG}.

Various techniques have been developed to reduce the stray capacitance in graphene devices, such as electrolyte gates [36], matching network circuits [37], and dispersive readout [38]. However, the technique in BLG devices has yet to mature, and there are few reports on it and not enough information about the resonator characteristics including the matching condition. Among them, reducing the size of the capacitance formed by the gate electrode is a simple approach. Such an approach has been reported for Si-based quantum dots [39–41]. In this work, we realize rf reflectometry in BLG devices utilizing microscale graphite back-gates to reduce the stray capacitance. We demonstrate the operation of reflectometry including the matching condition, and calculate the readout error rate of an electrostatically coupled charge sensor. Furthermore, Coulomb diamonds are observed through rf reflectometry. We consider that quantum dots are formed in the conduction channel by potential fluctuations by bubbles [42,43]. These are important in exploring the quantum dynamics in BLG and applications like quantum information processing.

II. DEVICE AND DC CHARACTERISTICS

Figure 1 shows the fabricated device structure. The device consists of layered two-dimensional materials: a graphite back-gate, a hexagonal boron nitride (*h*-BN) gate insulator, BLG flakes, and another *h*-BN gate insulator from bottom to top as shown in Fig. 1(a). This layered material is placed on top of the undoped Si substrate. The structure is prepared by the Elvacite transfer method [44]. On top of the structure, a 2-μm-wide Ti/Au top gate is placed on the top *h*-BN layer and Ti/Au source and drain contacts are prepared on BLG. Figure 1(b) shows a photograph of the device taken with an optical microscope. The long dotted line indicates BLG, and the short dotted line indicates the graphite back-gate. Important points of this device are the use of undoped Si substrates and microscale graphite back-gates to make the stray capacitance as small as possible. When a sample is placed on a conventional SiO_2/doped-Si substrate, the capacitance between the contact electrodes and the back-gate becomes large, and the rf signal used for reflectometry leaks to the back-gate. By using an undoped Si substrate, the parasitic capacitance is reduced and we are able to create a sample that can be used in rf reflectometry measurement.

Figure 1(c) shows the conductance of the BLG when dual gate voltages on the top gate (V_{TG}) and the back-gate (V_{BG}) are applied. In this measurement, the device is probed by direct current (dc) using a source measurement unit. The measurement temperature is 4.2 K. A low-conductance region appears in the diagonal direction. The total gate voltage V_{TG}+V_{BG} controls the Fermi level, and setting the level at close to the band gap leads to a low conductance. The slope of the diagonal low-conductance region is not unity because there are differences in the electrostatic coupling between V_{TG} and BLG, and V_{BG} and BLG. Also, the width of the low-conductance region reflects the opening of the band gap in BLG. The gap is opened by an electric field $\propto |V_{TG} - V_{BG}|$ [1], resulting in the width being very narrow near the origin. The opening of the band gap and accompanying pinch-off properties are observed. Note that other conductance decreases are observed in horizontal and vertical directions in the graph. Due to the device structure, there are regions where only the top or back gate covers and this induces additional decreases in the conductance. This behavior has been previously reported in a similar device structure [6]. One of the possible reasons for the shift of the charge-neutral point in graphene devices is caused by carrier doping from metal contacts [45].

III. RF REFLECTOMETRY

A. Resonance property

Next, we measure the resonance property of a resonator that includes the BLG device. The rf tank circuit is formed

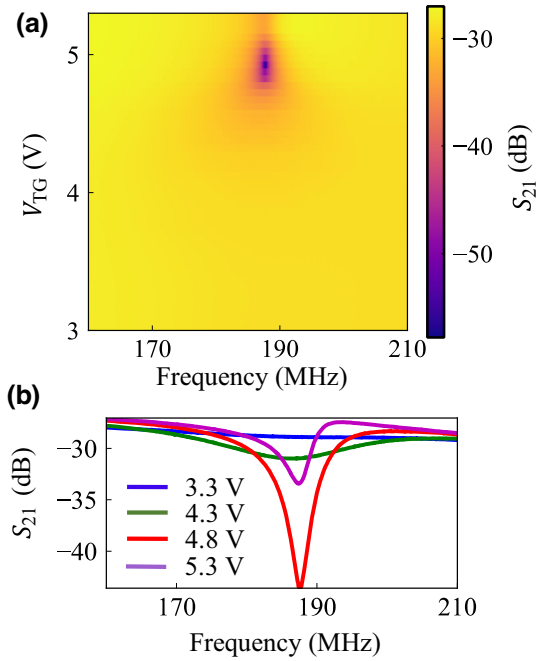

FIG. 2. (a) Observed S_{21} as a function of the frequency and V_{TG}. V_{BG} is fixed to -8 V in this measurement. The resonance changes with V_{TG}. (b) Resonance properties at $V_{TG} = 3.3, 4.3, 4.8$, and 5.3 V.

by a chip inductor $L = 1.2$ μH, a parasitic capacitor in the circuit C_p, and the graphene device as shown in Fig. 1(b). We measure the reflected signal from the resonator by a network analyzer through a directional coupler and an amplifier held at 4.2 K. Figure 2(a) shows the observed transmission coefficients S_{21} as a function of the frequency and V_{TG}. Note that S_{21} is measured by the input signal and reflected signal from the resonator by using a directional coupler, indicating that means the reflection coefficients. In this measurement, V_{BG} is fixed to -8 V. We observe the resonance around $f_{res} = 187.6$ MHz and the resonance is modified by the change of the device conductance through V_{TG}.

Figure 2(b) shows the resonance traces when $V_{TG} = 3.3, 4.3, 4.8$, and 5.3 V. The change of the resonance around $V_{TG} = 5$ V is consistent with the pinch-off property observed in Fig. 1(c). The reflected rf signal is modified and rf reflectometry operation is confirmed. The parasitic capacitance is evaluated as $C_p = 0.60$ pF, which mainly comes from the parasitic capacitance formed in the measurement board. The capacitance expected in the BLG device is calculated as 5.4 fF from the geometry. This value is small compared with 0.60 pF and will not greatly affect the observed resonance.

B. Demodulator measurement

We construct a demodulator circuit utilizing a mixer as shown in Fig. 3(a). The rf signal divided by the splitter is

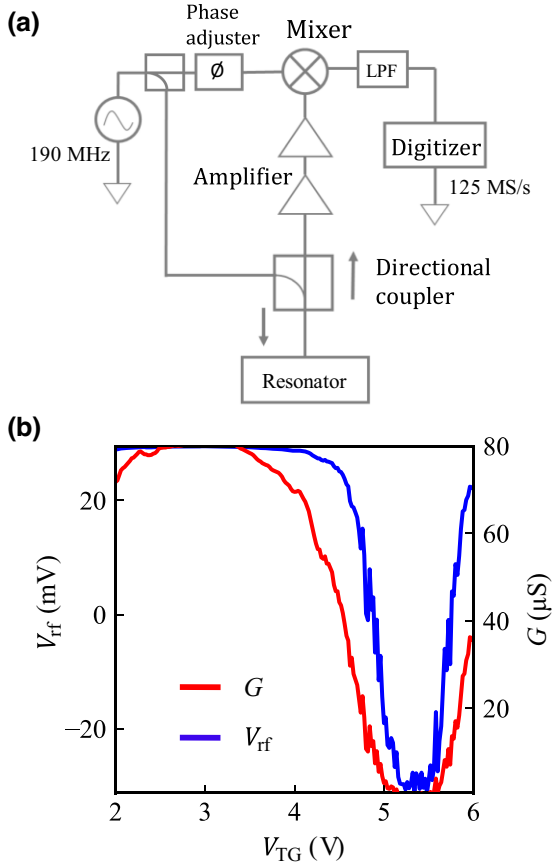

FIG. 3. (a) Schematic of the demodulator circuit utilizing a mixer for rf reflectometry. (b) Observed readout signal V_{rf} and the dc conductance G as a function of V_{TG}.

injected into the tank circuit including the sample through the directional coupler. The reflected signal is amplified and multiplied with the phase-adjusted input wave, and the resulting voltage through a low-pass filter (1.9 MHz) is measured by a digitizer. We optimize the phase adjuster and the rf signal power [46].

Figure 3(b) shows the the demodulated signal V_{rf} and the dc conductance G as a function of V_{TG}. The changes of V_{rf} and G are synchronized and we can detect the change of G by monitoring V_{rf}. Note that the observed nonlinearity between V_{rf} and G reflects the nonlinear relation in the reflection coefficient and G.

C. Noise analysis

We analyze the readout noise in rf reflectometry. Figures 4(a)–4(c) show the noise spectrum at $V_{TG} = 5.25, 4.8$, and 4.6 V, respectively. The spectra are calculated by fast Fourier transform of the real-time data. In this measurement, we remove the low-pass filter in Fig. 3(a). At $V_{TG} = 5.25$ and 4.8 V, we observe the same frequency dependence with rf reflectometry previously reported in GaAs quantum dots [47]. The solid red lines in Figs. 4(a) and 4(b) are the

fitting curve of the following equation:

$$V_{\mathrm{FFT}}(f) = \frac{\alpha}{f^{1/2}} - L_{\mathrm{S}}(f) + \text{offset}. \tag{1}$$

Here, α is the amplitude of the flicker noise corresponding to the device noise, $L_{\mathrm{S}}(f)$ is the symmetric Lorentz function to the circuit noise from the characteristics of the resonator and the amplifier, and the offset is the intrinsic noise of the amplifier. On the other hand, such behavior is not observed at 4.6 V in Fig. 4(c). The second term, $-L_{\mathrm{S}}(f)$, reproduces $V_{\mathrm{FFT}}(f)$ increasing with rf frequency around 10^6 Hz. This increase is not observed at 4.6 V in Fig. 4(c), indicating that rf reflectometry is insensitive in this voltage region. Therefore, we do not fit such noise spectra. This is because the conductance in such a region makes the resonator impedance far away from the matching conditions and the reflection coefficient is no longer sensitive to changes of the conductance. The dc measurement shows that the matching condition is satisfied with $G \sim 20$ μS at $V_{\mathrm{TG}} \sim 4.8$ V, where V_{rf} is close to zero. The reflection coefficient is sensitive enough to detect conductance changes in the pinch-off region, where the conductance becomes lower than 20 μS. This is important for applications to high-sensitivity single-charge detectors utilizing quantum point contacts and quantum dots, which usually operate at low-conductance conditions [33,35].

Furthermore, a positive correlation between α and $\left|\frac{dV_{\mathrm{rf}}}{dV_{\mathrm{TG}}}\right|$ is obtained as shown in Fig. 4(d). This relationship indicates that the flicker noise is caused by charge fluctuation near the channel in BLG. Note that there are a few points in the gray region away from the trend. This is because we calculate $\left|\frac{dV_{\mathrm{rf}}}{dV_{\mathrm{TG}}}\right|$ by a simple numerical differential of the measured data, which leads to spurious values resulting from the interplay of the measurement resolution and the fine signal oscillation, such as seen in Fig. 3(b). The signal oscillation corresponds to formation of quantum dots and is discussed in a later section. The present discussion shows that V_{rf} accurately reflects the operation of rf reflectometry and enables us to explain the noise mechanism of this measurement technique.

Next, we calculate the readout error rate of our BLG charge sensor for single-electron-transition detection if we couple the sensor to target quantum dots. From the noise analysis, we obtain the noise distribution σ to be 28 mV. The change in V_{rf} by single-electron transition is calculated by $V_{\mathrm{C}}\left|\frac{dV_{\mathrm{rf}}}{dV_{\mathrm{TG}}}\right|$, where V_{C} is the effective gate voltage through electrostatic coupling between the sensor and target quantum dots. Our BLG device has sensitivity $\left|\frac{dV_{\mathrm{rf}}}{dV_{\mathrm{TG}}}\right|$ of 0.25, and the signal-to-noise ratio (SNR) can be defined as $\mathrm{SNR} = \frac{V_{\mathrm{C}}}{\sigma}\left|\frac{dV_{\mathrm{rf}}}{dV_{\mathrm{TG}}}\right|$. The readout error rate can be described as $0.5\mathrm{erfc}(\mathrm{SNR}/2\sqrt{2})$ assuming a Gaussian noise distribution. Note that we can consider only Gaussian noise because other noise components, as mentioned above, are not dominant in the high-frequency domain we discuss here. For improvement of the SNR, the formation of a controllable quantum dot for the charge sensor is a promising solution because of the expected high sensitivity $\left|\frac{dV_{\mathrm{rf}}}{dV_{\mathrm{TG}}}\right|$. Figure 4(e) shows the V_{C} dependence of the readout error rate with various integration times $t_{\mathrm{int}} = 8$, 80, and 800 ns. Time integration is a noise reduction technique, which decreases σ by $1/\sqrt{N}$. Here, N is the number of integration samples that can be obtained from t_{int} and sampling

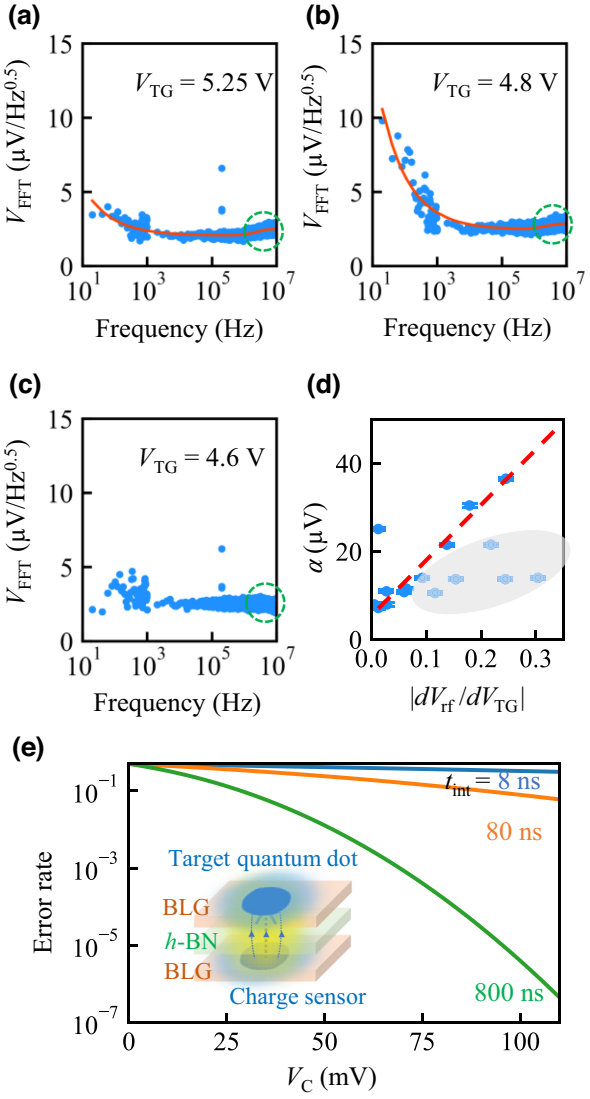

FIG. 4. Noise spectra at (a) $V_{\mathrm{TG}} = 5.25$ V, (b) 4.8 V, and (c) 4.6 V. The green dashed circles indicate the focus point to observe the effect of the resonator. (d) Correlation between α and $\left|\frac{dV_{\mathrm{rf}}}{dV_{\mathrm{TG}}}\right|$. The dashed red line is drawn as a guide to the eye. (e) V_{C} dependence of the calculated readout error rate. Blue, orange, and green lines correspond to $t_{\mathrm{int}} = 8$, 80, and 800 ns, respectively. The inset shows the concept of the charge sensor structure for high sensitivity.

frequency and the readout error rate decreases owing to the time integration.

The error rate can be further decreased if we can enhance V_C. In GaAs quantum dots [47,48], the value of V_C is about 1–10 mV. V_C is limited by the distance between the charge sensor and the target quantum dots and the screening by separator gate electrodes. In order to avoid these problems in two-dimensional material devices, a vertical configuration of the charge sensor shown as an inset in Fig. 4(e) can be expected. This type of structure has already been demonstrated experimentally to explore the current induced by back-action [49]. In this structure, the sensor and targets are physically separated whereas they are very close to the atomic-layer scale. The electrostatic coupling is inversely proportional to the distance, and we can expect a value of V_C of about 10–100 mV by assuming the difference in distance is an order of magnitude smaller compared with GaAs quantum dot devices. A previous study [49] also shows $V_C \sim 45$ mV between the top and bottom quantum dots, such a value being extracted from the stability diagrams. At a glance, large electrostatic coupling leading to a low readout error rate is expected in this structure. This concept can be applied to not only BLG but also other two-dimensional material-based devices.

D. Coulomb diamond

Finally, we use rf reflectometry to observe the quantum dots unintentionally created in the device. Figure 5(a) shows V_{rf} near the pinch-off of the BLG. Ideally, V_{rf} should show a smooth decrease due to the band gap caused by the vertical electric field. However, V_{rf} shows oscillations in addition to the background decrease. These oscillations are also observed in dc measurements as shown in Fig. 3(b), and can be identified as Coulomb peaks. The observed V_{rf} as a function of the source-drain bias V_{SD} and V_{TG} is shown in Fig. 5(b). The signal is also modulated by V_{SD} and Coulomb diamonds are observed (dashed lines). A possible mechanism for the formation of quantum dots is potential fluctuations due to air bubbles formed when the BLG is encapsulated with the boron nitride. In order to examine this scenario, we calculate the size of the formed quantum dot from the size of the Coulomb diamond. The smallest Coulomb peak interval at zero bias is 5 mV, corresponding to a gate capacitance of 32 aF. By assuming the quantum dots are circular, the radius of the dots is calculated to be 150 nm. This value is in good agreement with the bubble size in *h*-BN/graphene structures reported in previous works [50]. The band gap of BLG depends on the vertical electric field. Due to the thickness of the bubbles [42,43], the vertical electric field is modulated and quantum dots are created. These bubbles may be manipulated by an atomic force microscope (AFM) [51], which indicates that the quantum dot in our device can be controlled.

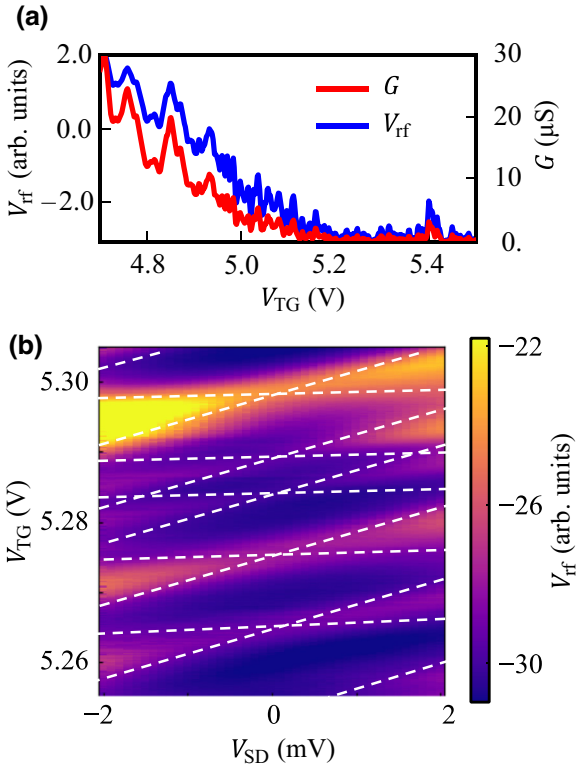

FIG. 5. (a) Enclosed trace of V_{rf} as a function of V_{TG}. (b) Observed V_{rf} as a function of the source-drain bias V_{SD} and V_{TG}.

IV. CONCLUSION

In conclusion, rf reflectometry in bilayer graphene devices is demonstrated by creating a device with a microscale graphite back-gate on an undoped Si substrate. The resonance property of the device connected to the tank circuit is measured using a network analyzer. We confirm that the matching condition close to the operating point can be maintained. This condition is important in sensitive quantum device readout [52]. We construct a demodulated rf reflectometry setup and the observed result shows good agreement with the dc measurement. The wide-range frequency-dependent noise property of rf reflectometry and the expected readout error rate in charge detection are evaluated and we demonstrate that a vertically integrated charge sensor has the potential to achieve a low error rate by utilizing a large electrostatic coupling for two-dimensional materials. We also measure Coulomb diamonds of quantum dots possibly formed by bubbles and confirm that rf reflectometry of quantum dots can be performed. Our results enable high-speed measurements of bilayer graphene quantum dot devices and aid the evaluation of bilayer graphene-based quantum bits by fast readout of the states. Furthermore, this work is expected to lead to investigation of the dynamics of valleytronics phenomena, opening up a new era in electronics.

ACKNOWLEDGMENTS

The authors thank S. Masubuchi, T. Machida, S. Alka, T. Kitada, T. Kumasaka, J. Llandro, and RIEC Fundamental Technology Center and the Laboratory for Nanoelectronics and Spintronics for fruitful discussions and technical support. Part of this work is supported by MEXT Leading Initiative for Excellent Young Researchers, Grants-in-Aid for Scientific Research (20H00237, 21K18592), Fujikura Foundation Research Grant, Hattori Hokokai Foundation Research Grant, Kondo Zaidan Research Grant, Tanigawa Foundation Research Grant, and FRiD Tohoku University.

[1] Y. Zhang, T.-T. Tang, C. Girit, Z. Hao, M. C. Martin, A. Zettl, M. F. Crommie, Y. R. Shen, and F. Wang, Direct observation of a widely tunable bandgap in bilayer graphene, Nature **459**, 820 (2009).

[2] C. R. Dean, A. F. Young, I. Meric, C. Lee, L. Wang, S. Sorgenfrei, K. Watanabe, T. Taniguchi, P. Kim, and K. L. Shepard, *et al.*, Boron nitride substrates for high-quality graphene electronics, Nat. Nanotechnol. **5**, 722 (2010).

[3] S. Moriyama, D. Tsuya, E. Watanabe, S. Uji, M. Shimizu, T. Mori, T. Yamaguchi, and K. Ishibashi, Coupled quantum dots in a graphene-based two-dimensional semimetal, Nano Lett. **9**, 2891 (2009).

[4] J. Güttinger, J. Seif, C. Stampfer, A. Capelli, K. Ensslin, and T. Ihn, Time-resolved charge detection in graphene quantum dots, Phys. Rev. B **83**, 165445 (2011).

[5] C. Volk, S. Fringes, B. Terrés, J. Dauber, S. Engels, S. Trellenkamp, and C. Stampfer, Electronic excited states in bilayer graphene double quantum dots, Nano Lett. **11**, 3581 (2011).

[6] M. Eich, F. Herman, R. Pisoni, H. Overweg, A. Kurzmann, Y. Lee, P. Rickhaus, K. Watanabe, T. Taniguchi, M. Sigrist, T. Ihn, and K. Ensslin, Spin and valley states in gate-defined bilayer graphene quantum dots, Phys. Rev. X **8**, 031023 (2018).

[7] A. Kurzmann, H. Overweg, M. Eich, A. Pally, P. Rickhaus, R. Pisoni, Y. Lee, K. Watanabe, T. Taniguchi, and T. Ihn, *et al.*, Charge detection in gate-defined bilayer graphene quantum dots, Nano Lett. **19**, 5216 (2019).

[8] A. Kurzmann, M. Eich, H. Overweg, M. Mangold, F. Herman, P. Rickhaus, R. Pisoni, Y. Lee, R. Garreis, and C. Tong, *et al.*, Excited States in Bilayer Graphene Quantum Dots, Phys. Rev. Lett. **123**, 026803 (2019).

[9] L. Banszerus, S. Möller, E. Icking, K. Watanabe, T. Taniguchi, C. Volk, and C. Stampfer, Single-electron double quantum dots in bilayer graphene, Nano Lett. **20**, 2005 (2020).

[10] L. Banszerus, K. Hecker, E. Icking, S. Trellenkamp, F. Lentz, D. Neumaier, K. Watanabe, T. Taniguchi, C. Volk, and C. Stampfer, Pulsed-gate spectroscopy of single-electron spin states in bilayer graphene quantum dots, Phys. Rev. B **103**, L081404 (2021).

[11] L. Banszerus, S. Möller, C. Steiner, E. Icking, S. Trellenkamp, F. Lentz, K. Watanabe, T. Taniguchi, C. Volk, and C. Stampfer, Spin-valley coupling in single-electron bilayer graphene quantum dots, Nat. Commun. **12**, 1 (2021).

[12] S. Tarucha, D. Austing, T. Honda, R. Van der Hage, and L. P. Kouwenhoven, Shell Filling and Spin Effects in a Few Electron Quantum Dot, Phys. Rev. Lett. **77**, 3613 (1996).

[13] L. P. Kouwenhoven, T. Oosterkamp, M. Danoesastro, M. Eto, D. Austing, T. Honda, and S. Tarucha, Excitation spectra of circular few-electron quantum dots, Science **278**, 1788 (1997).

[14] L. P. Kouwenhoven, D. Austing, and S. Tarucha, Few-electron quantum dots, Rep. Prog. Phys. **64**, 701 (2001).

[15] R. Hanson, L. P. Kouwenhoven, J. R. Petta, S. Tarucha, and L. M. K. Vandersypen, Spins in few-electron quantum dots, Rev. Mod. Phys. **79**, 1217 (2007).

[16] D. Loss and D. P. DiVincenzo, Quantum computation with quantum dots, Phys. Rev. A **57**, 120 (1998).

[17] J. R. Petta, A. C. Johnson, J. M. Taylor, E. A. Laird, A. Yacoby, M. D. Lukin, C. M. Marcus, M. P. Hanson, and A. C. Gossard, Coherent manipulation of coupled electron spins in semiconductor quantum dots, Science **309**, 2180 (2005).

[18] F. H. L. Koppens, C. Buizert, K. J. Tielrooij, I. T. Vink, K. C. Nowack, T. Meunier, L. P. Kouwenhoven, and L. M. K. Vandersypen, Driven coherent oscillations of a single electron spin in a quantum dot, Nature **442**, 766 (2006).

[19] T. D. Ladd, F. Jelezko, R. Laflamme, Y. Nakamura, C. Monroe, and J. L. O'Brien, Quantum computers, Nature **464**, 45 (2010).

[20] M. Veldhorst, C. H. Yang, J. C. C. Hwang, W. Huang, J. P. Dehollain, J. T. Muhonen, S. Simmons, A. Laucht, F. E. Hudson, K. M. Itoh, A. Morello, and A. S. Dzurak, A two-qubit logic gate in silicon, Nature **526**, 410 (2015).

[21] T. Otsuka, T. Nakajima, M. R. Delbecq, S. Amaha, J. Yoneda, K. Takeda, G. Allison, T. Ito, R. Sugawara, A. Noiri, A. Ludwig, A. D. Wieck, and S. Tarucha, Single-electron spin resonance in a quadruple quantum dot, Sci. Rep. **6**, 31820 (2016).

[22] J. Yoneda, K. Takeda, T. Otsuka, T. Nakajima, M. R. Delbecq, G. Allison, T. Honda, T. Kodera, S. Oda, Y. Hoshi, N. Usami, K. M. Itoh, and S. Tarucha, A quantum-dot spin qubit with coherence limited by charge noise and fidelity higher than 99.9%, Nat. Nanotechnol. **13**, 102 (2018).

[23] C. Altimiras, H. le Sueur, U. Gennser, A. Cavanna, D. Mailly, and F. Pierre, Tuning Energy Relaxation Along Quantum Hall Channels, Phys. Rev. Lett. **105**, 226804 (2010).

[24] T. Otsuka, S. Amaha, T. Nakajima, M. R. Delbecq, J. Yoneda, K. Takeda, R. Sugawara, G. Allison, A. Ludwig, A. D. Wieck, and S. Tarucha, Fast probe of local electronic states in nanostructures utilizing a single-lead quantum dot, Sci. Pep. **5**, 14616 (2015).

[25] T. Otsuka, T. Nakajima, M. R. Delbecq, P. Stano, S. Amaha, J. Yoneda, K. Takeda, G. Allison, S. Li, A. Noiri, T. Ito, D. Loss, A. Ludwig, A. D. Wieck, and S. Tarucha, Difference in charge and spin dynamics in a quantum dot–lead coupled system, Phys. Rev. B **99**, 085402 (2019).

[26] B. Trauzettel, D. V. Bulaev, D. Loss, and G. Burkard, Spin qubits in graphene quantum dots, Nat. Phys. **3**, 192 (2007).

[27] J. Velasco Jr, J. Lee, D. Wong, S. Kahn, H.-Z. Tsai, J. Costello, T. Umeda, T. Taniguchi, K. Watanabe, and A. Zettl, *et al.*, Visualization and control of single-electron charging in bilayer graphene quantum dots, Nano Lett. **18**, 5104 (2018).

[28] Z. Ge, F. Joucken, E. Quezada, D. R. Da Costa, J. Davenport, B. Giraldo, T. Taniguchi, K. Watanabe, N. P. Kobayashi, and T. Low, *et al.*, Visualization and manipulation of bilayer graphene quantum dots with broken rotational symmetry and nontrivial topology, Nano Lett. **20**, 8682 (2020).

[29] Y.-W. Liu, Z. Hou, S.-Y. Li, Q.-F. Sun, and L. He, Movable Valley Switch Driven by Berry Phase in Bilayer-Graphene Resonators, Phys. Rev. Lett. **124**, 166801 (2020).

[30] Y.-N. Ren, Q. Cheng, Q.-F. Sun, and L. He, Realizing Valley-Polarized Energy Spectra in Bilayer Graphene Quantum Dots via Continuously Tunable Berry Phases, Phys. Rev. Lett. **128**, 206805 (2022).

[31] R. Schoelkopf, P. Wahlgren, A. Kozhevnikov, P. Delsing, and D. Prober, The radio-frequency single-electron transistor (rf-set): A fast and ultrasensitive electrometer, Science **280**, 1238 (1998).

[32] H. Qin and D. A. Williams, Radio-frequency point-contact electrometer, Appl. Phys. Lett. **88**, 203506 (2006).

[33] D. Reilly, C. Marcus, M. Hanson, and A. Gossard, Fast single-charge sensing with a rf quantum point contact, Appl. Phys. Lett. **91**, 162101 (2007).

[34] C. Barthel, D. Reilly, C. M. Marcus, M. Hanson, and A. Gossard, Rapid Single-Shot Measurement of a Singlet-Triplet Qubit, Phys. Rev. Lett. **103**, 160503 (2009).

[35] C. Barthel, M. Kjærgaard, J. Medford, M. Stopa, C. M. Marcus, M. P. Hanson, and A. C. Gossard, Fast sensing of double-dot charge arrangement and spin state with a radio-frequency sensor quantum dot, Phys. Rev. B **81**, 161308 (2010).

[36] W. Fu, M. El Abbassi, T. Hasler, M. Jung, M. Steinacher, M. Calame, C. Schönenberger, G. Puebla-Hellmann, S. Hellmüller, and T. Ihn, *et al.*, Electrolyte gate dependent high-frequency measurement of graphene field-effect transistor for sensing applications, Appl. Phys. Lett. **104**, 013102 (2014).

[37] T. Müller, J. Güttinger, D. Bischoff, S. Hellmüller, K. Ensslin, and T. Ihn, Fast detection of single-charge tunneling to a graphene quantum dot in a multi-level regime, Appl. Phys. Lett. **101**, 012104 (2012).

[38] L. Banszerus, S. Möller, E. Icking, C. Steiner, D. Neumaier, M. Otto, K. Watanabe, T. Taniguchi, C. Volk, and C. Stampfer, Dispersive sensing of charge states in a bilayer graphene quantum dot, Appl. Phys. Lett. **118**, 093104 (2021).

[39] A. Noiri, K. Takeda, J. Yoneda, T. Nakajima, T. Kodera, and S. Tarucha, Radio-frequency-detected fast charge sensing in undoped silicon quantum dots, Nano Lett. **20**, 947 (2020).

[40] R. Mizokuchi, S. Bugu, M. Hirayama, J. Yoneda, and T. Kodera, Radio-frequency single electron transistors in physically defined silicon quantum dots with a sensitive phase response, Sci. Rep. **11**, 1 (2021).

[41] S. Bugu, S. Nishiyama, K. Kato, Y. Liu, T. Mori, and T. Kodera, Rf reflectometry for readout of charge transition in a physically defined p-channel mos silicon quantum dot, Jpn. J. Appl. Phys. **60**, 1 (2021).

[42] D. A. Bahamon, Z. Qi, H. S. Park, V. M. Pereira, and D. K. Campbell, Conductance signatures of electron confinement induced by strained nanobubbles in graphene, Nanoscale **7**, 15300 (2015).

[43] N. Leconte, H. Kim, H.-J. Kim, D. H. Ha, K. Watanabe, T. Taniguchi, J. Jung, and S. Jung, Graphene bubbles and their role in graphene quantum transport, Nanoscale **9**, 6041 (2017).

[44] S. Masubuchi, M. Morimoto, S. Morikawa, M. Onodera, Y. Asakawa, K. Watanabe, T. Taniguchi, and T. Machida, Autonomous robotic searching and assembly of two-dimensional crystals to build van der Waals superlattices, Nat. Commun. **9**, 1413 (2018).

[45] R. Nouchi, T. Saito, and K. Tanigaki, Determination of carrier type doped from metal contacts to graphene by channel-length-dependent shift of charge neutrality points, Appl. Phys. Express **4**, 035101 (2011).

[46] See Supplemental Material at http://link.aps.org/supplemental/10.1103/PhysRevApplied.20.014035 for the parameter optimization of the phase adjuster and the rf signal power.

[47] M. Shinozaki, Y. Muto, T. Kitada, T. Nakajima, M. R. Delbecq, J. Yoneda, K. Takeda, A. Noiri, T. Ito, and A. Ludwig, *et al.*, Gate voltage dependence of noise distribution in radio-frequency reflectometry in gallium arsenide quantum dots, Appl. Phys. Express **14**, 035002 (2021).

[48] R. Schleser, E. Ruh, T. Ihn, K. Ensslin, D. Driscoll, and A. Gossard, Time-resolved detection of individual electrons in a quantum dot, Appl. Phys. Lett. **85**, 2005 (2004).

[49] D. Bischoff, M. Eich, O. Zilberberg, C. Rössler, T. Ihn, and K. Ensslin, Measurement back-action in stacked graphene quantum dots, Nano Lett. **15**, 6003 (2015).

[50] R. Frisenda, E. Navarro-Moratalla, P. Gant, D. P. De Lara, P. Jarillo-Herrero, R. V. Gorbachev, and A. Castellanos-Gomez, Recent progress in the assembly of nanodevices and van der Waals heterostructures by deterministic placement of 2d materials, Chem. Soc. Rev. **47**, 53 (2018).

[51] M. R. Rosenberger, H.-J. Chuang, K. M. McCreary, A. T. Hanbicki, S. V. Sivaram, and B. T. Jonker, Nano-"squeegee" for the creation of clean 2d material interfaces, ACS Appl. Mater. Interfaces **10**, 10379 (2018).

[52] F. Vigneau, F. Fedele, A. Chatterjee, D. Reilly, F. Kuemmeth, M. F. Gonzalez-Zalba, E. Laird, and N. Ares, Probing quantum devices with radio-frequency reflectometry, Appl. Phys. Rev. **10**, 021305 (2023).